NANO LETTERS

2009
Vol. 9, No. 4
1341-1344

Axial p-n Junctions Realized in Silicon Nanowires by Ion Implantation

S. Hoffmann,[†] J. Bauer,[‡] C. Ronning,[§] Th. Stelzner,[||] J. Michler,[†] C. Ballif,[⊥] V. Sivakov,[‡,||] and S. H. Christiansen*[,‡,||]

Laboratory for Mechanics of Materials and Nanostructures, Empa Materials Science and Technology, Feuerwerkstrasse 39, 3602 Thun, Switzerland, Max Planck Institute of Microstructure Physics, Weinberg 2, 06120 Halle, Germany, Institute of Solid State Physics, University of Jena, Max-Wien-Platz 1, 07743 Jena, Germany, Institute of Photonic Technology, AlbertEinsteinStrasse 9, 07745 Jena, Germany, and Institute of Microtechnology, University of Neuchatel, A.-L. Breguet 2, 2000 Neuchatel, Switzerland

Received October 1, 2008; Revised Manuscript Received January 18, 2009

ABSTRACT

The electrical properties of vertically aligned silicon nanowires doped by ion implantation are studied in this paper by a combination of electron beam-induced current imaging and two terminal current−voltage measurements. By varying the implantation parameters in several process steps, uniform p- and n-doping profiles as well as p-n junctions along the nanowire axis are realized. The effective doping is demonstrated by electron beam-induced current imaging on single nanowires, and current−voltage measurements show their well-defined rectifying behavior.

Semiconductor nanowires are expected to play a critical role in future electronic devices and sensors.[1] To make use of their semiconducting properties, doping is an important issue. Nanowires that form an epitaxial interface and thus are vertically aligned to the substrate are commonly grown by the vapor−liquid−solid (VLS) mechanism in which a metal catalyst forms eutectic droplets at the growing tips of the nanowires.[2] For silicon nanowires, a supply of Si vapor supersaturates these droplets with Si and leads to its precipitation at the liquid−solid (droplet−silicon) interface. Under the gold droplet, the nanowire grows as long as the Si vapor is present. Silicon nanowires reveal p-type conductance when they are grown using the VLS process without adding any dopant on purpose, but the resistivity is rather high (2 Ω cm^3−400 Ω cm^4).

Doping can be realized during the gas phase deposition process by adding dopants to the gas mixture in use for the nanowire growth. Dopant incorporation is reported for diborane,[4] trimethylboron,[5] phosphine,[3] and arsenic.[6] By changing the dopant source during growth, p-n junctions can be realized along the axis of the nanowire.[6,7] Little is known on the dopant incorporation mechanism, however. Therefore, it is not obvious to predict the doping concentration for a given process. Also, recent experimental results reveal the growth of a highly doped shell around the nanowire while doping during VLS growth.[8]

As an alternative, reproducible and successful doping of nanowires can be achieved via ion implantation. This technique is a standard doping technique in top−down semiconductor manufacturing and offers the advantage to provide for precise control over the total dose of dopants, depth profile, and most importantly works well also for high doping levels of the order of 10^{20}−10^{21} cm^{-3}. It has been demonstrated that GaAs can be p-type doped using Zn ions, and Si by the respective use of B and P ions.[10] The latter work presents field effect transistors based on ion-implanted nanowires. However, the demonstration of ion-implanted nanowires acting as devices by themselves is still lacking. Masking selected parts of the sample at different implantation steps, the doping profile can be chosen to be different from nanowire to nanowire. This is an additional advantage over doping during growth, or etching nanowires out of a doped wafer, as for both these methods all nanowires reveal the same doping concentration.

This paper presents post-growth doping of nominally undoped VLS silicon nanowires by ion implantation. By varying the fluencies, acceleration voltages, and ions in subsequent implantation steps, uniform n- and p-type doping as well as p-n profiles are achieved along the nanowire axis. Electron beam-induced current (EBIC) imaging demonstrates

* To whom correspondence should be addressed. E-mail: sechrist@mpi-halle.mpg.de.
[†] Empa Materials Science and Technology.
[‡] Max Planck Institute of Microstructure Physics.
[§] University of Jena.
[||] Institute of Photonic Technology.
[⊥] University of Neuchatel.

10.1021/nl802977m CCC: $40.75
Published on Web 03/03/2009

the successful activation of the dopants, and current−voltage ($I-V$) characteristics show the rectifying behavior of the p-n junctions.

Nanowires are grown by Au-catalyzed VLS growth by electron beam evaporation,[11−13] where the gaseous silicon source is provided from atomic silicon evaporated by electron beam irradiation. The substrates, all (111)-orientated wafers, are chosen to match the doping type of the bottom of the nanowires. Details on the growth process can be found in ref 11 (summary can be found in Supporting Information). The resulting vertically aligned nanowires are 250−500 nm long and 150−400 nm in diameter. Compared to other VLS grown nanowires, ours are relatively wide. Wide nanowires have a potential application in photovoltaics. Nanowire solar cells are found to have a higher light absorption than thin films, and cells with wide nanowires show a higher efficiency than cells with thinner ones.[14]

A hopping conductivity across gold agglomerates on the nanowire sidewalls was measured on similarly grown nanowires,[15] therefore special care is taken to remove the gold droplets atop the nanowires and on the nanowire sidewalls. Therefore, gold agglomeration to bigger clusters on the surfaces is supported by annealing the samples at 800 °C for 15 min in air, and subsequently the silicon oxide is removed by a 2% HF dip for 2 min. Immediately after the HF dip, the sample is immersed in aqua regia in order to etch away the gold agglomerates. Scanning electron microscope (SEM) investigations show that the large Au droplets atop the nanowire and smaller droplets on the nanowire sidewalls are entirely removed after this treatment. Transmission electron microscopy studies, however, reveal in rare cases that very small Au agglomerates are still presented on the nanowires.[16]

Ion implantation of $^{11}B^+$ (as acceptor) and $^{31}P^+$ (as donor) is performed at room temperature with ion energies varying from 1 to 400 keV and fluxes between $0.05-3 \times 10^{14}$ cm^{-2}. The sample surface is aligned almost perpendicular with respect to the ion beam, thus, the vertically aligned nanowires face the ion beam. An angle of a few degrees is used in order to avoid channeling effects into the <111> axis. The detailed implantation profiles are calculated with the program package TRIM[17] (Supporting Information). The maximum implantation depth matches the length of the nanowires and the peak concentration of each dopant reaches $1-1.5 \times 10^{19}$ cm^{-3}. All three samples are annealed directly after implantation at 850 °C for 15 min in order to remove the implantation damage.[18] The pressure is kept below 1.5×10^{-6} mbar during annealing, avoiding oxidation of the Si substrate and nanowires.

The results on three different samples are presented (see Figure 1), the first purely n-doped (sample 1), the second n-doped at the top and p-doped at the bottom (sample 2) and the third p-doped at the top and n-doped at the bottom (sample 3). The silicon substrate is n-type (P, 120 Ω cm) for samples 1 and 3 and p-type (B, 10 Ω cm) for sample 2. An SEM image of a nanowire together with an overview over the different doping schemes is given in Figure 1, and

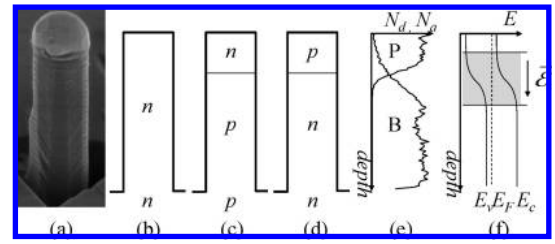

Figure 1. (a) SEM image of a silicon nanowire with the gold catalyst still on top. (b−d) Doping scheme for samples 1−3. (e) Simulated doping profile of sample 2. (f) Corresponding band structure; the depletion region is gray shaded and the direction of the electric field indicated.

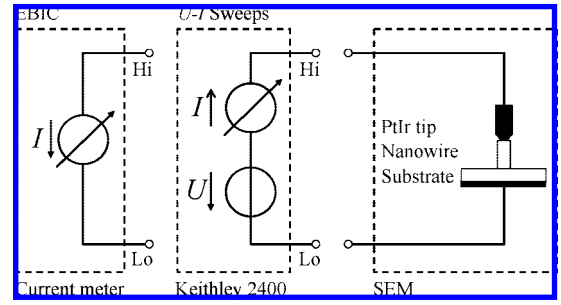

Figure 2. The electrical connections to the nanowire for imaging the EBIC and measuring the current−voltage characteristics.

the detailed doping profile is given in the Supporting Information.

Electrical characterization of nanowires is commonly done by dispersing them on an isolating substrate and contacting them by electron beam lithography. This works well to contact nanostructures when the requirement on the alignment precision is in the order of a few 100 nm or above. Below 200 nm, the yield drops drastically, and in addition the rather thick nanowires require thick electrodes, which puts constraints on the minimum lateral feature size. As an alternative to lithography, a conductive PtIr tip mounted on a nanomanipulator setup inside an SEM is being used to directly contact the nanowires that grow perpendicular to the substrate surface. The substrate serves as the second contact. Details on the nanomanipulator setup can be found in ref 19, and the etching process for the PtIr tip is described in the Supporting Information.

The principle of EBIC is based on the electric field present in the depletion region of a Schottky or p-n junction.[20] The electron beam of the SEM is scanning over the sample, inducing electron−hole pairs in the semiconductor. In absence of an electric field, these eventually recombine. But if the induced charge carriers diffuse into the depletion region of a junction (gray in Figure 1f), the electric field separates them which leads to a net current when the circuit is closed. The magnitude of the induced current at each pixel is represented by different gray levels in the EBIC image. For orientation, the EBIC image is always shown next to a secondary electron (SE) image of the same location and with the same magnification.

Figure 2 shows the electrical scheme for the EBIC imaging and for performing the $I-V$ sweeps. As an example, in this

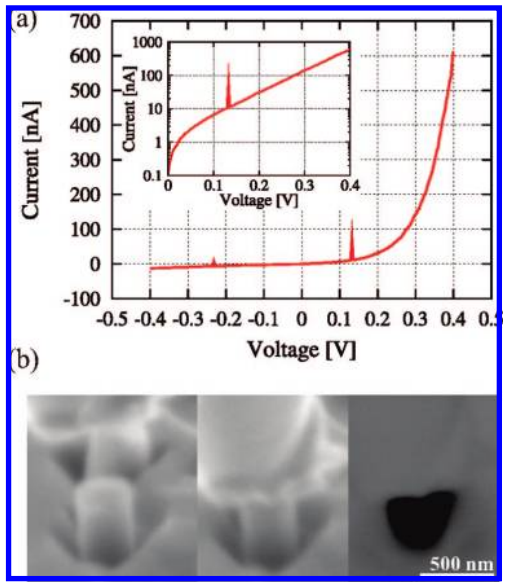

Figure 3. (a) Current−voltage characteristic of a PtIr tip in contact with a uniformly n-doped nanowire from sample 1. (b) (Left) SE image of the nanowire under investigation; (center) SE image of the tip in contact with the nanowire; (right) EBIC image of the Schottky contact at the tip−nanowire interface. The nanowires are standing at an angle of 60° with respect to the electron beam.

configuration a positive EBIC current (reverse bias current) is expected for a Schottky contact between the PtIr tip and the n-doped nanowire of sample 1, because electrons drift to the nanowire and holes to the tip. A positive current is represented by dark pixels in the EBIC image.

Figure 3 shows an $I-V$ curve and an EBIC image of a uniformly n-doped nanowire from sample 1. As expected, the EBIC signal is located at the tip−nanowire contact and black, indicating a positive current. The current−voltage characteristic is rectifying with the forward direction from the tip to the nanowire. The current follows the equation

$$I = I_0(e^{\frac{qV}{\eta kT}} - 1) \qquad (1)$$

and from the logarithmic plot in the inset one can extract a quality factor of $\eta = 2.6$.

The EBIC images of samples 2 and 3 are shown in Figure 4a,b, respectively. As expected, a negative current represented by a white spot demonstrates the n-p (top−bottom) junction in the nanowire from sample 2, and the inverse contrast is revealed in sample 3. All the current−voltage sweeps performed on these nanowires show the rectifying nature of the junctions, but they differ in magnitude. Figure 5a shows a sweep performed on a nanowire from sample 2. The inset shows that the increase in current in forward bias is not exponential; it is thus not possible to extract a quality factor. The sweeps performed on a nanowire from sample 3, plotted in Figure 5b, demonstrate the rectifying behavior as well, but the magnitude in current differs for different tip−nanowire contact areas. Although most current is present in the first sweep (red, solid curve), it decreases drastically when the contact area is small (center image in the inset, green, dashed curve), and increases again when the contact area is larger (right inset, blue, dotted curve).

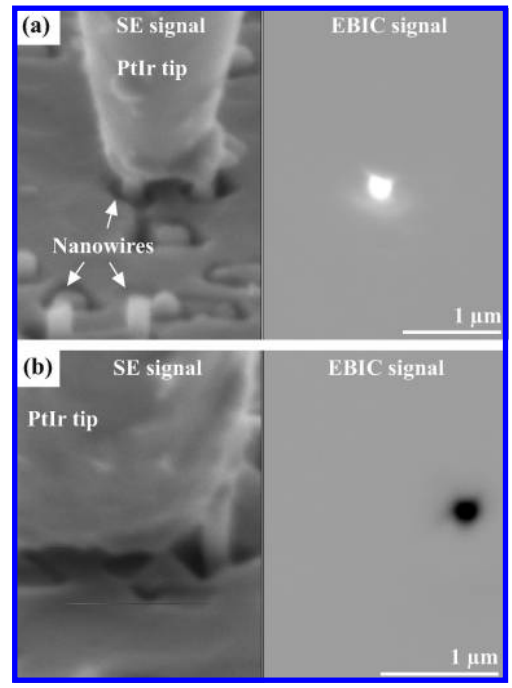

Figure 4. SE and EBIC images of (a) n-p nanowires (sample 2) and (b) p-n nanowires (sample 3). The nanowires are standing at an angle of 60° with respect to the electron beam.

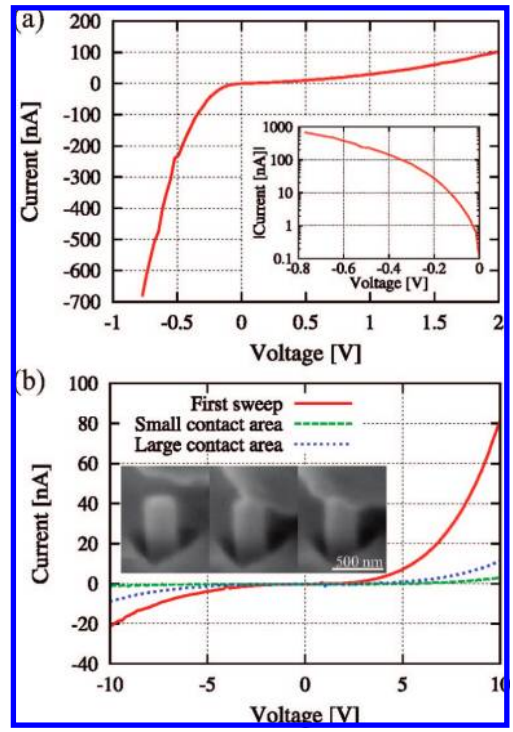

Figure 5. Current−voltage characteristics measured on p-n-doped nanowires. (a) Nanowire from sample 2, the same as from which the EBIC image is taken in Figure 4a. (b) A nanowire from sample 3, shown in the left inset. The red, solid curve shows the first recorded sweep, the green, dashed curve shows the second sweep with only a small contact area between tip and nanowire (center inset), and the blue, dotted curve shows the sweep with a larger contact area (right inset).

During the ion implantation process, half of the sample area is masked so that the nanowires underneath the mask remain undoped. EBIC images of those nanowires show a faint EBIC signal between the nanowire and the substrate (not shown here), as it has been observed on undoped nanowires already.[15] The current through an undoped nanowire in the $I-V$ sweeps is 2−3 orders of magnitudes lower than through a doped nanowire, demonstrating that the nanowires conductance increases upon ion beam doping.

The EBIC images reveal the expected doping and junctions and thus proof the effective doping of the nanowires. This observation is also supported by the measured $I-V$ curves. In agreement with ref 10, ion implantation is a suitable tool to fabricate functional devices from as grown nanowires.

For the p-n-doped nanowires, it is not possible to tell where exactly the junction is located; it can, however, be excluded that the EBIC signal originates from a Schottky contact at the tip−nanowire interface. Such a Schottky contact would reveal an inverse contrast, black for the tip n-doped top of the nanowire from sample 2 and white for the tip p-doped top of the nanowire from sample 3.

The current−voltage characteristics of the Schottky contact on the nanowire of sample 1 reveals the expected rectifying behavior, and its steepest slope shows that the series resistance is smaller than 60 kΩ. This resistance however is not necessarily linked to the nanowire. The spreading resistance through the substrate is in that order of magnitude, too. For a top contact area with diameter d (diameter of the nanowire), a substrate resistivity ρ, a substrate thickness h, and a bottom contact area $\gg h^2$, the spreading resistance R_{sp} is[21]

$$R_{sp} = \frac{\rho}{\pi d} \tan^{-1}\left(\frac{4h}{d}\right) \quad (2)$$

With a substrate thickness of 0.58 cm, a substrate resistivity of 120 Ω cm, and a nanowire diameter of 380 nm, this yields a spreading resistance of 13−260 kΩ. This cannot be neglected, so the two point measurement does not allow to calculate the resistivity of the nanowire.

The quality factor η (eq 1) ideally is $\eta = 1$ for a Schottky diode when dominated by thermionic emission. Tunneling through the barrier increases η,[21] and the measured quality factor of 2.6 thus indicates qualitatively that the doping concentration is $>10^{18}$ cm^{-3}. For the targeted doping concentration of 1.3×10^{19} cm^{-3}, the thermionic field emission is the dominant process. For doping concentrations above 10^{20} cm^{-3}, field emission would be the dominant process and one would expect a linear $I-V$ characteristic (ohmic contact). The effective doping concentration thus lies between $10^{18}-10^{20}$ cm^{-3} according to the electrical results and is thus matching the desired concentration from the ion implantation process.

The current of the nanowire from sample 2 becomes linear with respect to the voltage for $U < -0.5$ V, and the series resistance extracted from this experiment is 625 kΩ. With a nanowire diameter of 190 nm and a substrate doping concentration of 10 Ω cm, the spreading resistance through the substrate is about 300 kΩ cm. It is thus not possible to extract an accurate series resistance of the nanowire in this sample either. Neither is it possible for the nanowire of sample 3, as there it is the tip−nanowire contact area which is limiting the current.

In conclusion it is demonstrated that nanowires can effectively be doped by ion implantation, and functional devices can be realized. By implanting in several steps with different implantation parameters, uniform doping profiles as well as p-n junctions are achieved. The successful activation of the dopants is demonstrated by EBIC imaging and two point current−voltage measurements.

Acknowledgment. C.R. and S.C. acknowledge financial funding by DFG Grant Ro1198/72,3 and CH159/61, respectively. S.H. acknowledges financial support by the European Commission (FP6, NanoHand, No. 034274, IST).

Supporting Information Available: This material is available free of charge via the Internet at http://pubs.acs.org.

References

(1) Lu, W.; Lieber, C. M. *J. Phys. D: Appl. Phys.* **2006**, *39*, R387.
(2) Givargizov, E. I. *J. Cryst. Growth* **1975**, *31*, 20.
(3) Wang, Y.; Lew, K. K.; Ho, T. T.; Pan, L.; Novak, S. W.; Dickey, E. C.; Redwing, J. M.; Mayer, T. S. *Nano Lett.* **2005**, *5*, 2139.
(4) Cui, Y.; Duan, X.; Hu, J.; Lieber, C. *J. Phys. Chem. B* **2000**, *104*, 5213.
(5) Lew, K. K.; Pan, L.; Bogart, T. E.; Dilts, S. M.; Dickey, E. C.; Redwing, J. M.; Wang, Y.; Cabassi, M.; Mayer, T. S.; Novak, S. W. *Appl. Phys. Lett.* **2004**, *85*, 3101.
(6) Tang, Q.; Kamins, T. I.; Liu, X.; Grupp, D. E.; Harrisa, J. S. *Electrochem. Solid-State Lett.* **2005**, *8*, G240.
(7) Gudiksen, M. S.; Lauhon, L. J.; Wang, J.; Smith, D. C.; Lieber, C. M. *Nature* **2002**, *415*, 617.
(8) Imamura, G.; Kawashima, T.; Fujii, M.; Nishimura, C.; Saitoh, T.; Hayashi, S. *Nano Lett.* **2008**, *8*, 2620.
(9) Stichtenoth, D.; Wegener, K.; Gutsche, C.; Regolin, I.; Tegude, F. J.; Prost, W.; Seibt, M.; Ronning, C. *Appl. Phys. Lett.* **2008**, *92*, 163107.
(10) Colli, A.; Fasoli, A.; Ronning, C.; Pisana, S.; Piscance, S.; Ferrari, A. C. *Nano Lett.* **2008**, *8*, 2188.
(11) Sivakov, V.; Heyroth, F.; Falk, F.; Andrä, G.; Christiansen, S. *J. Cryst. Growth* **2007**, *300*, 288.
(12) Sivakov, V.; Andrae, G.; Gösele, U.; Christiansen, S. H. *Phys. Status Solidi A* **2007**, *203*, 3692.
(13) Sivakov, V.; Stelzner, T.; Andrae, G.; Gösele, U.; Christiansen, S. H. *Appl. Phys. A* **2006**, *85*, 311.
(14) Hu, L.; Chen, G. *Nano Lett.* **2007**, 3249.
(15) Bauer, J.; Fleischer, F.; Breitenstein, O.; Schubert, L.; Werner, P.; Gösele, U.; Zacharias, M. *Appl. Phys. Lett.* **2007**, *90*, 012105.
(16) Christiansen, S. H.; Chou, J. W.; Becker, M.; Sivakov, V.; Ehrhold, K.; Berger, A.; Chou, W. C.; Chuu, D. S.; Gösele, U. *Nanotechnology* **2009**, accepted for publication.
(17) Ziegler, J. F.; Biersack, J. P.; Littmark, U. *The stopping and ranges of ions in solids*; Pergamon Press: Elmsford, NY, 1985.
(18) Mayer, J. W.; Eriksson, L.; Davies, J. A. *Ion implantation into Semiconductors*; Academic Press: New York, 1970.
(19) Hoffmann, S.; Utke, I.; Moser, B.; Michler, J.; Christiansen, S. H.; Schmidt, V.; Senz, S.; Werner, P.; Gösele, U.; Ballif, C. *Nano Lett.* **2006**, *6*, 622.
(20) Leamy, H. J. *J. Appl. Phys.* **1982**, *53*, R51.
(21) Sze, S. M.; Ng, K. K. *Physics of semiconductor devices*, 3rd ed; John Wiley and Sons: New York, 2007.
(22) Libioulle, L.; Houbion, Y.; Gilles, J.-M. *Rev. Sci. Instrum.* **1995**, *66*, 97.

NL802977M